5D.2 MULTISCALE STRUCTURE AND EVOLUTION OF EARL (2010) DURING RAPID INTENSIFICATION

Robert Rogers[1]*, Paul Reasor[1], and Jun Zhang[2]
[1]NOAA/AOML Hurricane Research Division
[2]University of Miami/Cooperative Institute for Marine and Atmospheric Studies

1. INTRODUCTION

Progress in tropical cyclone (TC) intensity forecasts has lagged that of track forecasts (Rogers et al. 2013a; DeMaria et al. 2005), largely because of the multiscale nature of the processes responsible for intensity change (Marks and Shay 1998). Some skill at predicting rapid intensification has been attained by using algorithms that rely primarily on environmental-scale parameters (Kaplan et al. 2010). However, there is much room for improvement, suggesting that processes operating on scales smaller than the environmental scale also contribute to intensity change (Hendricks et al. 2010).

Vortex, convective, and boundary layer processes have been examined as subsynoptic-scale contributors to RI. Symmetric vortex-scale processes involved with TC intensification involve the cooperative interaction between the symmetric primary and secondary circulation patterns and the impact of axisymmetric diabatic heating on this interaction, while asymmetric processes such as vertical wind shear and eye-eyewall mixing have also been identified as important contributors to intensification. Convection and its role in RI has focused primarily on the role of convective bursts (CBs). The exact role that CBs play has been tied to warming from upper-level subsidence around the periphery of the bursts and to the stretching and subsequent axisymmetrization of low-level vorticity collocated with the updraft in vortical hot towers. Boundary-layer impacts on RI have focused on two modes of radial inflow: a deep, relatively weak inflow that converges absolute angular momentum above the boundary layer, where it is conserved; and strong inflow in the lowest 1 km that also converges angular momentum and creates supergradient flow as the inflowing air converges absolute angular momentum at a rate that exceeds its dissipation to the ocean surface via friction.

Using composites of airborne Doppler measurements, Rogers et al. (2013b, hereafter R13) compared the vortex- and convective-scale structure of hurricanes that intensify with those that remain steady-state. Statistically-significant vortex-scale differences were identified in R13, including ring-like axisymmetric vorticity inside the radius of maximum wind (RMW); lower vorticity in the outer core; deeper, stronger inflow;

stronger axisymmetric eyewall upward motion; and a greater azimuthal coverage of precipitation for intensifying hurricanes. On the convective scale, R13 found that the primary difference was a higher concentration of CBs inside the RMW for intensifying hurricanes, consistent with balance arguments relating the efficiency with which diabatic heating released within the storm core is converted into an increase in the kinetic energy of the storm. While these composite results show relationships in a statistically robust manner, only TCs of hurricane strength were included. Also, composites lack the temporal continuity to provide information on the mechanisms underlying the relationships mentioned above.

In this study a set of observations from Hurricane Earl (2010) will be presented. Earl underwent RI in the western Atlantic in August 2010. It was intensively sampled by a multitude of aircraft during most of its lifetime (Rogers et al. 2013a, Braun et al. 2013, Montgomery et al. 2014, Uhlhorn et al. 2014), including the NOAA WP-3D and G-IV, NASA DC-8 and Global Hawk, and Air Force C-130 aircraft. The NOAA WP-3D aircraft sampled Earl at 12-h intervals beginning before RI, when it was a 25 m s^{-1} tropical storm, during RI, and at the end of RI ~60 h later, when it was a ~55 m s^{-1} Category 3 hurricane (Fig. 1). The temporal coverage provided by these flights provides an opportunity to study the impact of CBs on the onset and subsequent extended period of RI.
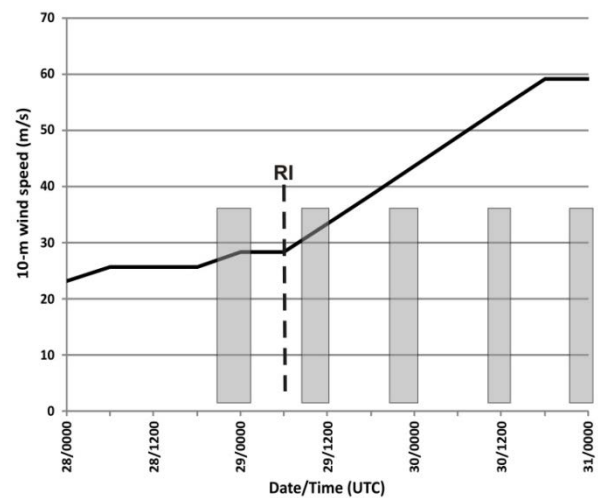

Figure 1. Best Track intensity for Earl (m s^{-1}). Approximate on-station times of WP-3D missions indicated by grey boxes. Onset of RI indicated by bold dashed line.

---

*Corresponding author e-mail: Robert.Rogers@noaa.gov

1

2. DATASET

The analysis presented here relies primarily on data obtained from the X-band tail Doppler radar onboard the NOAA WP-3D aircraft. Analyses from this data are derived from a variational algorithm that simultaneously solves the continuity and Doppler projection equations using least-squares minimization (Gamache 1997, Reasor et al. 2009) to produce grids with horizontal and vertical spacings of 2 km and 0.5 km, respectively. An automated version of this algorithm is used here, similar to that used in Stern and Nolan (2009, 2011), Rogers et al. (2012, R13), Reasor et al. (2013), Hazelton and Hart (2013), and DeHart et al. (2014). In addition to the Doppler analyses, GPS dropsondes are used to document the lower-level and boundary layer thermodynamic and kinematic structure of Earl.

3. OVERVIEW OF EARL'S RI

Earl developed from a strong tropical wave that emerged off the coast of Africa in late August 2010. The system was declared a tropical depression by the National Hurricane Center at 0600 UTC 25 August and within 6 h the system was declared a tropical storm. Earl moved toward the west and west-northwest at ~7 m s^{-1}, slowly intensifying during this time. By 1200 UTC 28 August, just prior to the first NOAA aircraft missions (Fig. 1), Earl had intensified to a moderate tropical storm of ~25 m s^{-1}. Over the next 24 h Earl slowed its forward motion and turned more toward the northwest, just to the northeast of the Leeward Islands. Just prior to the second WP-3D mission, around 0600 UTC 29 August, the intensification rate increased significantly. This is identified as the onset of RI. The best track intensity increased ~30 m s^{-1} during the next three missions, reaching ~60 m s^{-1} by 0000 UTC 31 August. The time period described here, i.e., prior to and during RI, is the focus of this study.

Earl's environment (not shown) was generally characterized by moderate 850-200 hPa shear (8 m s^{-1}) from the northeast during the first two WP-3D missions, decreasing by the third mission as Earl approaches major hurricane status. The sea-surface temperature is high during this time, with values between 29 and 30 C based on global model analyses. The low- to midlevel humidity was low around the periphery of Earl, but within the immediate environment the environment remained moist.

Radius-height cross sections of axisymmetric tangential wind and vorticity (Fig. 2) show that Earl's circulation is shallow during the first two missions, with the tangential wind maximum only extending up to ~6 km. A clear change in the vertical structure of Earl is seen by the third mission, as the tangential wind maximum extends to a higher altitude and the RMW has contracted. By the fourth and fifth missions, Earl is a well-developed hurricane with a deep, strong primary circulation. Outside the RMW the tangential winds increase during the third to fifth missions. The axisymmetric vorticity field is also shallow during the first two missions. By the third mission a core of high vorticity of 35 x 10^{-4} s^{-1} is seen within the inner 20 km. Additionally, there is a narrow band of higher vorticity along the inner edge of the tangential wind maximum, extending up to 9 km altitude. Such a ring-like structure in the vorticity field has been seen in previous observational studies of intensifying TC's (Kossin and Eastin 2001, R13), indicating a regime favorable for the horizontal mixing of vorticity between the eye and eyewall. The fourth mission indicates that this ring-like vorticity structure is even more pronounced. Additionally, vorticity outside the RMW has increased, particularly within the radial band ~2 x RMW. By the fifth mission the core vorticity peaks at >50 x 10^{-4} s^{-1} as the RMW has contracted to ~25 km. The vorticity outside the RMW (2-3 x RMW) has continued to increase, consistent with an expanding tangential wind field and the eventual development of a secondary eyewall after this time.
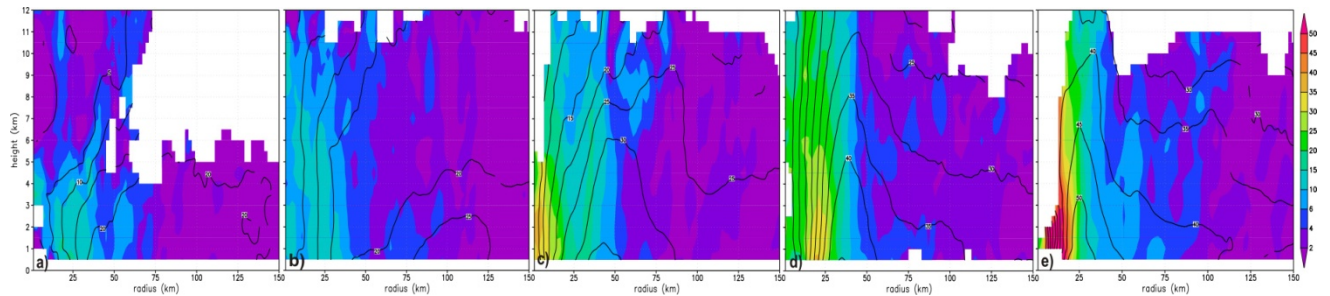

Figure 2. Radius-height cross sections of axisymmetric vorticity (shaded, x 10^{-4} s^{-1}) and axisymmetric tangential wind (contour, m s^{-1}) for missions (a) 100828I1; (b) 100829H1; (c) 100829I1; (d) 100830H1; and (e) 100830I1. Locations with more than 180 degrees of contiguous gap were not plotted.

The evolution of the symmetric structure described above indicates that there are two stages of Earl's RI. During the early stage, which lasts for the first two missions, the storm encounters moderate vertical shear and its symmetric circulation is shallow, broad, and diffuse. RI begins just prior to the second mission. During the subsequent three missions the shear drops and the vortex develops a deep primary symmetric circulation whose RMW contracts while intensifying to a major hurricane. The next section will discuss the inner-core structure and evolution of the vortex during these two stages, and the role that deep convection plays during each of the stages.

4. TWO STAGES OF EARL'S RI

a) Early stage: Alignment of circulation centers in moderate shear

During the first two missions Earl is characterized by a broad, shallow axisymmetric tangential wind and vorticity field (cf. Figs. 2). Figure 3 shows the storm-relative wind speed at 2 km and the circulation at 2, 5, and 8 km along with the large-scale (SHIPS-derived) 850-200 hPa shear and storm motion vectors at the nearest 6-h time to the first mission. The circulation center was nearly aligned between 2 and 5 km, though the circulation elongated toward the southeast at 5 km. At 8 km, the circulation center is displaced ~50 km to the east-southeast of the 2- and 5-km centers. The direction of displacement of the 8-km center is to the left of the northeasterly large-scale shear vector, consistent with what has been shown in theoretical, numerical, and observational studies of vortices in shear (e.g., Jones 1995, Wang and Holland 1996, Reasor and Eastin 2012, Reasor et al. 2013), though those studies primarily considered vortices of hurricane strength. By the time of the second mission 12 h later, the circulations were nearly aligned (not shown), despite the presence of moderate shear persisting from the northeast.
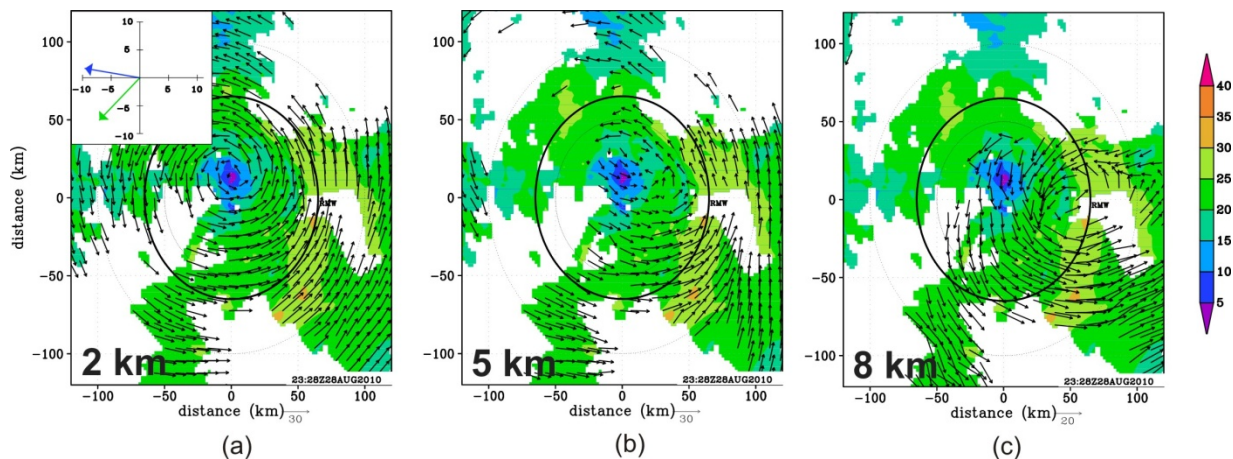

Figure 3. Storm-relative wind speed (shaded, m s^{-1}) at 2 km (2 km altitude in all panels) and flow vectors at indicated altitude (m s^{-1}) from merged analyses for mission 100828H1 at (a) 2 km; (b) 5 km; and (c) 8 km altitude. Inset on (a) shows the SHIPS-derived 850-200 hPa shear vector (green arrow, m s^{-1}) and storm motion vector (blue arrow, m s^{-1}) for the 6-h time nearest to the mission.

The evolution of the vortex during the first mission can be seen by examining the individual radial passes that comprise the merged analyses from Fig. 3. Figure 4 shows the storm-relative flow at 8 km, radar reflectivity at 2 km, and locations of CBs for radial passes during the first mission (centered at 2129 and 2254 UTC 28 and 0125 UTC 29 August). CBs here are defined as those locations where the maximum vertical velocity in the 8-16 km layer is > 5 m s^{-1} and the reflectivity averaged in the 8-14 km layer is > 20 dBZ. These criteria were chosen to capture those convective features with strong updrafts in the middle to upper troposphere that transport high reflectivity aloft, similar to the hot tower structures seen in previous spaceborne and airborne studies (e.g., Heymsfield et al. 2001, Cecil et al. 2002, Kelley et al. 2004, Guimond et al. 2010). These deep convective cores, representing the top 1% of the vertical velocity distribution above the freezing level sampled by airborne Doppler radar near the RMW, were found to be a key convective-scale feature distinguishing intensifying from steady-state hurricanes as shown in R13.

An asymmetric distribution of high reflectivity and CB activity is apparent during the three passes, with the heaviest precipitation and most vigorous upper-level updrafts confined to the east side of the storm, i.e., left
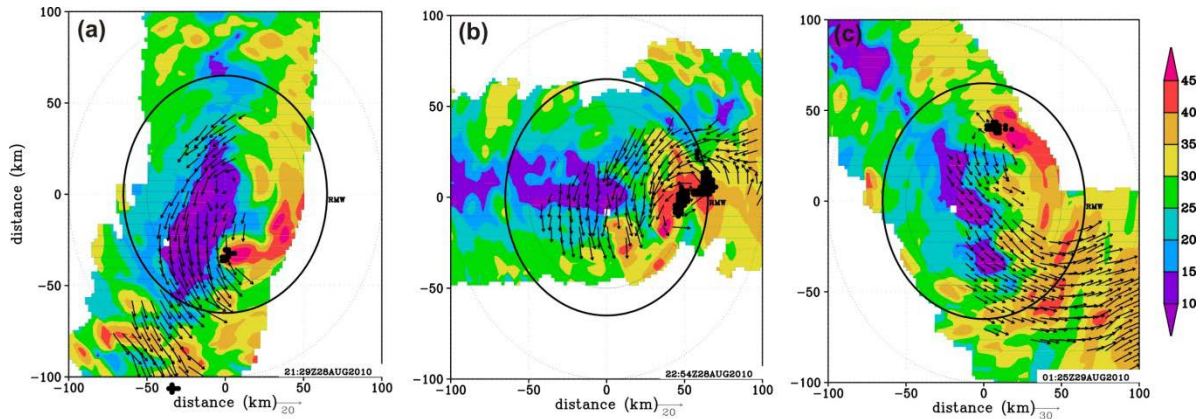
Figure 4. (a) Reflectivity (shaded, dBZ) at 2-km altitude from tail Doppler radar during individual radial pass through Earl centered at 2129 UTC 28 August. Vectors (m s⁻¹) show storm-relative flow at 8 km. Black dots denote locations of points flagged as convective bursts. RMW at 2-km altitude indicated by circle; (b) As in (a), but for pass centered at 2254 UTC 28 August; (c) As in (a), but for pass centered at 0125 UTC 29 August. Domains in all images are 200 km on a side.

of the deep-layer shear vector (cf. Fig. 4a). The primary CB activity is concentrated inside the RMW at the tip of a band that spirals out toward the south and southwest of the center, with some isolated grid points flagged as CBs at these larger radii. The CB activity inside the RMW is seen from both the tail Doppler and LF radars to translate from the southeast to the northeast side of the storm during the ~4 h period covered by these radial passes, passing through an arc left of the shear vector in a manner consistent with that shown in Black et al. (2002). The flow vectors at 8 km show a clear cyclonic curvature associated with the convective burst. While the limited coverage of the wind field near the edges of the analyses precludes a definitive determination of the center location of the cyclonic curvature for each individual pass, it does appear that the center of the cyclonic feature approximately translates with the motion of the burst. This suggests that the region of cyclonic curvature at 8 km and vigorous convection are linked. From these analyses it is clear that the onset of RI is tied to the alignment of the vortex by the second mission. Additionally, the CB's (and their associated mesoscale convective system) likely played a role in causing the vortex alignment.

b) Late stage: Convective bursts located inside RMW

By the time of the third mission, Earl was well into its RI period (cf. Fig. 1) and was now a category 1 hurricane of ~35 m s⁻¹. The structure at this time consisted of a deep primary circulation and an RMW of ~50 km that contracted to < 25 km between the third and fifth missions (Fig. 2). Figure 5 shows the storm-relative flow field and reflectivity at 2 km and CB locations from selected radial passes from each of the next three missions. The bulk of the eyewall convection remains located left of the shear vector, even as the

shear vector changes from being northeasterly to northwesterly from the third to the fifth flight. The radius of the peak eyewall convection, similar to the RMW, contracts during the three missions. The vortex shows 2-8 km tilt values < 5 km throughout this time (not shown).

The distribution of CB's as a function of normalized radius is shown in Fig. 6 for both the early and late stages of Earl's RI. During the early stage the CB's are broadly distributed across radial bands inside r = 1.5 x RMW, with a distinct peak inside r = 0.5 x RMW. During the late stage the distribution of CB's becomes much more concentrated around the RMW, as the secondary circulation becomes better established and provides a stronger constraint on the radial location of deep convection. The peak CB activity remains inside the RMW, i.e., between the r = 0.75 and 1 x RMW radial band, consistent with the composite results of intensifying hurricanes shown in R13. As mentioned above, dynamically this radial location is important because the peak diabatic heating associated with these CB's is located inside the RMW, where the vorticity and inertial stability are high (cf. Fig. 3) and the heating thus has a comparatively large impact on TC intensification (Shapiro and Willoughby 1982; Schubert and Hack 1982; Nolan et al. 2007; Vigh and Schubert 2009; Pendergrass and Willoughby 2009).

As mentioned above, the peak in the distribution of CB's inside the RMW at 2 km for Earl is consistent with intensifying hurricanes, as shown in R13. For steady-state hurricanes, by contrast, the radial distribution of CB's is characterized by a peak outside the RMW at 2 km. A key question to ask is why this relationship exists. One possible explanation is convergence in the boundary layer. Figure 7 shows cross sections of
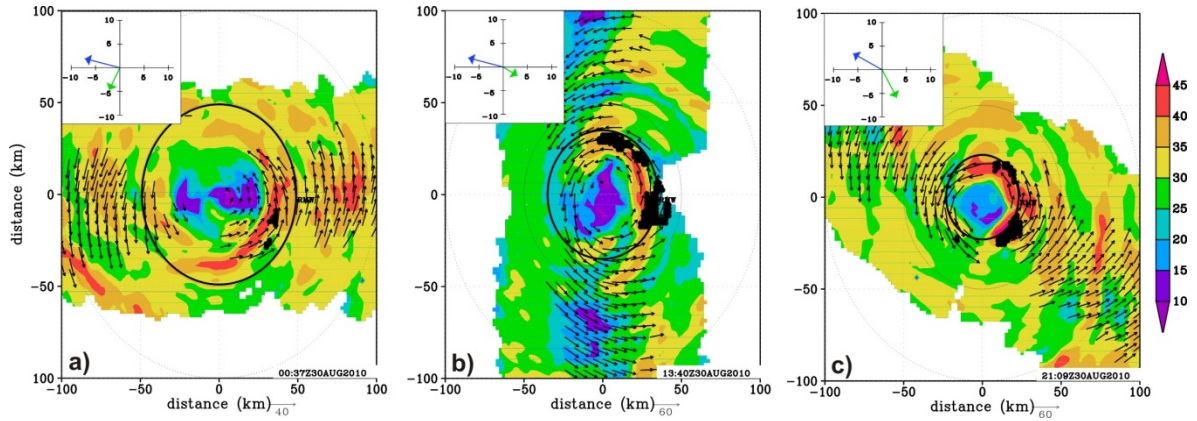
4

Figure 5. (a) Reflectivity (shaded, dBZ) at 2-km altitude from tail Doppler radar during individual radial pass through Earl centered at 0037 UTC 30 August. Vectors (m s⁻¹) show storm-relative 8-km flow. Black dots denote locations of points flagged as convective bursts. RMW at 2-km altitude indicated by circle; (b) As in (a), but for pass centered at 1340 UTC 30 August; (c) As in (a), but for pass centered at 2109 UTC 30 August; (Domains in all images are 200 km on a side. Insets show SHIPS-derived 850-200 hPa shear vector (green arrow, m s⁻¹) and storm motion vector (blue arrow, m s⁻¹) for 6-h time nearest to the mission.
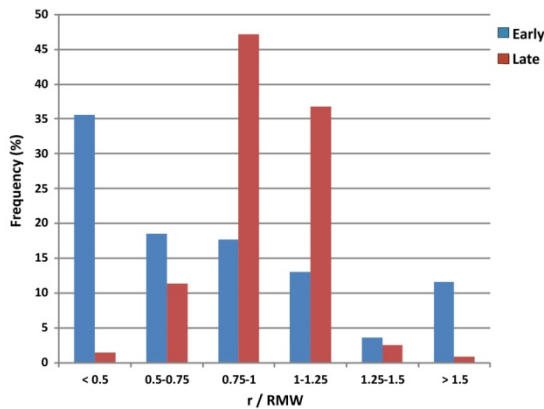

Figure 6. Radial distribution of convective bursts (frequency, %) as a function of radius relative to 2-km RMW for early stage (blue) and late stage (red).

boundary-layer axisymmetric tangential and radial wind, agradient wind, and the radial gradient of radial flow (a proxy for divergence in this framework) calculated from dropsondes from all aircraft from the 12-h period surrounding 00 UTC 30 August. This matches one of the time periods examined in Montgomery et al. (2014), who performed a study of the boundary-layer structure of Earl during its RI (see their Fig. 4b for a map of the dropsonde coverage). The tangential wind shows the RMW at around 40 km radius below 500 m altitude. Near-surface inflow values > 14 m s⁻¹ are seen at 75 km, or ~1.5 x RMW, providing a significant inward advection of angular momentum. The tangential flow inside the RMW is highly supergradient from the surface to 2 km (Fig. 7c). The radial gradient of radial flow (Fig. 7d) shows that the strongest convergence is below 500

m and is located inside the RMW, with peak values at around 0.3-0.5 x RMW. This indicates that the low-level forcing for eyewall convection is inside the RMW for this case. While boundary layer convergence was maximized inside the RMW for Earl, this mechanism
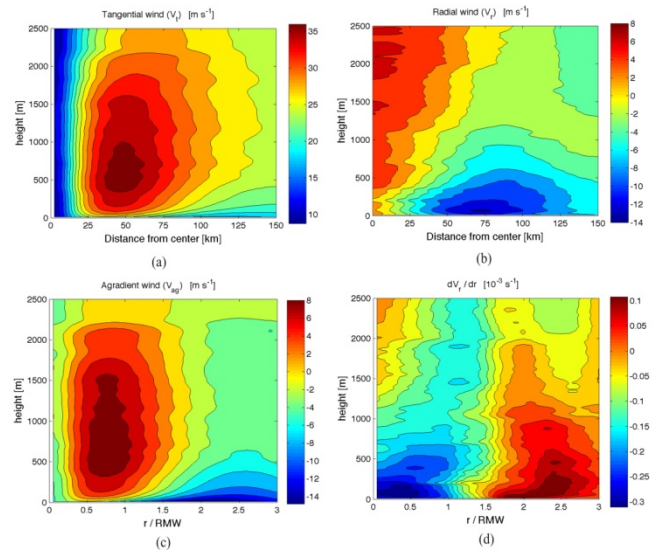

Figure 7. (a) Radius-height plot of axisymmetric tangential wind (shaded, m s⁻¹) from all dropsondes in a 12-h time window centered on 00 UTC 30 August; (b) As in (a), but for axisymmetric radial flow (shaded, m s⁻¹); (c) radius-height plot of agradient flow (shaded, m s⁻¹). Radius is normalized by radius of axisymmetric wind at 2 km; (d) As in (c), but for the radial gradient of axisymmetric radial wind (shaded, x 10-3 s⁻¹).

cannot be definitively identified as one that distinguishes intensifying from steady-state hurricanes. What is needed is sufficient dropsonde coverage in the 1-3 x RMW range for a steady-state hurricane with similar

characteristics to Earl to determine if convergence is maximized outside the RMW. Such a dataset is missing at this point.

5. RADIAL DISTRIBUTION OF CB'S: A COMPARISON OF AN INTENSIFYING AND STEADY-STATE CASE

In addition to the boundary layer convergence mechanism, R13 proposed other explanations for the difference in CB radial distribution between intensifying and steady-state hurricanes that do not require a dense coverage of dropsondes outside the RMW. One possibility is a reduced inertial stability outside the RMW in intensifying storms. Reduced outer-core inertial stability provides less resistance to radial displacements, resulting in a greater radial mass flux.

One way to test this hypothesis is to examine differences in the inner-core structure for two cases: one that had CB's inside the 2-km RMW and intensified, and another that had CB's primarily outside the RMW and remained steady-state. Figure 8 shows two such cases: the intensifying case is from the fourth mission in Earl, centered at ~12 UTC 30 August, and the steady-state case is Gustav, which was a ~42 m s^{-1} hurricane at
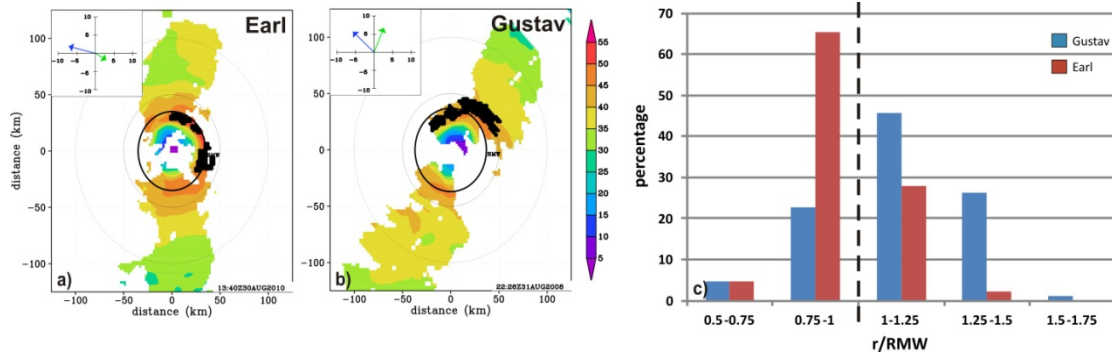

Figure 8. (a) Storm-relative wind speed (shaded, m s-1) at 2-km altitude for pass centered at 1340 UTC from mission 100830H1 in Hurricane Earl; (b) As in (a), but for pass centered at 2226 UTC from mission 100831H1 in Hurricane Gustav; (c) Normalized radial distribution of convective bursts for all passes from the missions in Earl and Gustav from (a) and (b). Dashed line in (c) denotes location of RMW. Insets on (a) and (b) show the SHIPS-derived shear vector (green arrow, m s^{-1}) and storm motion vector (blue arrow, m s-1) for the 6-h time nearest to the mission.

the time of the WP-3D mission centered at ~00 UTC 1 September 2008. Earl intensified 10 m s^{-1} in the 12 h time window centered on the mission, while Gustav's intensity did not change during this same window (not shown). Figure 8 shows 2 km wind speed and CB locations from a single pass, along with storm motion and 850-200 hPa vertical shear vectors, for the two missions. Both Gustav and Earl were tracking generally toward the west-northwest at ~7 m s^{-1}. Earl was encountering northwesterly shear < 5 m s^{-1}, while Gustav was encountering southwesterly shear of ~6 m s^{-1}. Both hurricanes had an RMW of ~35 km at the time of their respective missions. Earl had most of its CB's inside the 2-km RMW, whereas Gustav had a significant number of CB's outside the RMW. This relationship is further illustrated in Fig. 8c, which shows the radial distribution of CB's for all radial passes comprising the Earl and Gustav missions shown in Fig. 8a-b. Earl shows a peak in CB distribution between 0.75 and 1 x RMW, consistent with Fig. 8, while Gustav shows a peak in CB distribution between 1 and 1.25 x RMW.

Figure 9 shows radius-height plots of axisymmetric inertial stability, tangential wind, and radial wind for the Earl and Gustav missions. The tangential wind and inertial stability fields inside the RMW are similar between the two storms below 6 km. Above that height

the inertial stability is higher for Earl than Gustav. Outside the RMW, beginning at ~60 km radius (i.e., ~2 x RMW), the tangential wind field is stronger and the inertial stability is higher in Gustav than Earl. A higher outer-core inertial stability can result in weaker, shallower inflow (Kepert 2001), reducing the convergence of angular momentum surfaces in an axisymmetric sense and weakening the "conventional spin up" mechanism (Ooyama 1982, Montgomery et al. 2014). The axisymmetric radial flow shown in Fig. 9c-d indicates that this is indeed the case, as the depth and magnitude of the inflow layer is larger for Earl than Gustav.

Another possible explanation for the differences in the radial distribution of CBs is the slope of the updrafts associated with the CBs. Since the relationship between CB radial location and RMW considers the RMW at 2 km altitude, whereas the criteria identifying CB's consider the vertical velocity and reflectivity above 8 km, CB locations based on this algorithm are also dependent on the slope of the updraft. The placement of a CB outside the 2-km RMW could simply reflect an updraft that is sloped, even if it had its origin in the low-level convergent region inside the RMW (cf. Fig. 7). Figure 8 shows comparisons of vertical velocity, inertial stability, and tangential wind averaged around the
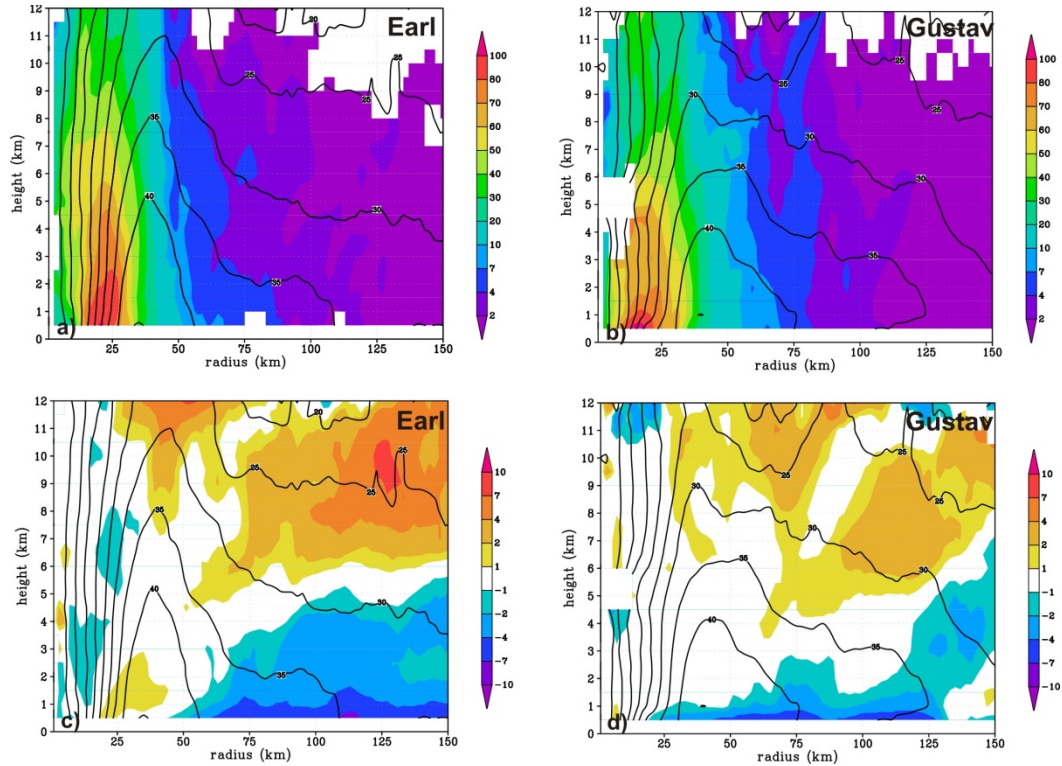
Figure 9. (a) Radius-height plot of axisymmetric inertial stability (I^2, shaded, x 10^{-7} s^{-2}) and tangential wind (contour, m s^{-1}) for mission 100830H1 in Earl; (b) As in (a), but for mission 080831H1 in Gustav; (c) Radius-height plot of axisymmetric radial flow (shaded, m s^{-1}) and tangential wind (contour, m s-1) for mission 100830H1 in Earl; (d) As in (c), but for mission 080831H1 in Gustav.

downshear side of Earl and Gustav. In addition, the angular momentum (M) surfaces passing through the 2-km RMW and axes of peak updrafts are marked. The slope of the M surfaces are similar for both Earl and Gustav. For both storms the peak updraft axis originates inside the 2-km RMW, consistent with the location of peak low-level convergence shown in Fig. 7 for Earl. Above the low levels, though, the slope of the updraft axis differs. For Earl the updraft axis is nearly vertical, whereas for Gustav the updraft axis slopes outward between 5 and 8 km altitude. Above 8 km the updraft axis for Gustav becomes nearly vertical again. The angle between the updraft axis and M surface is large for Earl, while for Gustav the updraft axis is nearly parallel to the M surface (up to 8 km). An updraft axis, and by extension an axis of diabatic heating, that is more upright than the M surface results in a greater convergence of angular momentum and vortex spin-up (Pendergrass and Willoughby 2009). Hazelton et al. (2014) found a similar relationship for intensifying and weakening hurricanes when they compared the slopes of reflectivity (which can be considered a proxy for updrafts) and M in the downshear left and upshear left quadrants. Another way to interpret this effect is to compare the location of the updraft axis with the local RMW (i.e., the RMW at the same height, rather than 2

km). For Earl the updraft axis remains inside the local RMW at all altitudes, while for Gustav the updraft axis crosses the local RMW at 7 km altitude and remains outside the RMW above. This results in the updraft axis for Earl being in a region of higher inertial stability throughout its ascent, compared with Gustav whose updraft axis extends into a region of lower inertial stability (cf. Figs. 10b,d) – a difference that results in a greater impact of the diabatic heating on Earl than for Gustav.

The differences between Earl and Gustav highlighted above provide additional possibilities to explain why CB's appear to be preferentially–located inside the 2-km RMW for intensifying hurricanes, whereas they are located outside the 2-km RMW for steady-state hurricanes. From the standpoint of updraft slope, the relevant question then becomes what causes updrafts to be more vertical in some cases and more sloped in others. One logical possibility is buoyancy of the boundary layer air flowing into the eyewall. Air with greater convective available potential energy would ascend more vigorously, departing from the local M surfaces and spinning up the vortex via the conventional method.
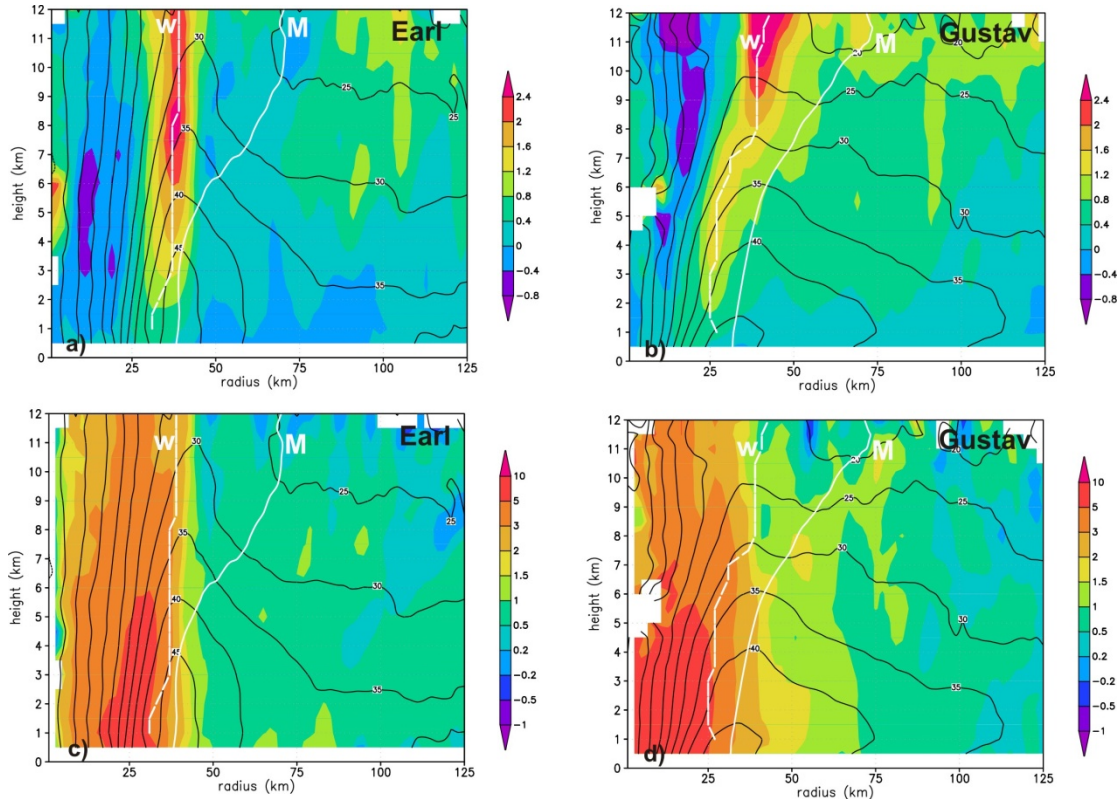
Figure 10. (a) Radius-height plot of vertical velocity (shaded, m s^{-1}) and tangential wind (contour, m s^{-1}) on the downshear side for mission 100830H1 in Earl; (b) As in (a), but for mission 080831H1 in Gustav; (c) Radius-height plot of inertial stability (I^2, shaded, x 10^{-7} s^{-2}) and tangential wind (contour, m s^{-1}) on the downshear side for mission 100830H1 in Earl; (d) As in (c), but for mission 080831H1 in Gustav. In all figures white solid line denotes angular momentum surface passing through 2-km RMW (marked with "M"); white dashed line denotes axis of peak updraft (marked with "w").

6. DISCUSSION AND CONCLUDING REMARKS

The results shown here have depicted the rapid intensification of Earl as occurring in two stages. During the early stage, the symmetric component of Earl was shallow, broad, and diffuse, and Earl was experiencing moderate northeasterly shear and had an asymmetric distribution of convection. During the first mission, the cyclonic circulation at 8 km was significantly displaced from the 2- and 5-km centers. There was a convective burst located on the east side of the storm that appeared to play a role in positioning a cyclonic circulation at 8 km above the low-level center. By the time of the second mission the vortex was aligned and extended over a deep layer, and rapid intensification had begun. During the late stage RI continued, as Earl intensified ~20 m s^{-1} in the 24-h period comprising this stage. The vortex remained generally aligned in the presence of weaker vertical shear. Convective bursts were noted near the RMW during each of the three flights comprising this stage, with the majority of the CB's located just inside the RMW. Each of the two stages described here raises questions about the role of vortex, convective, and boundary layer processes in rapid intensification.

For the early stage, the primary questions pertain to the role that the CB, and its associated mesoscale convective system, play in the alignment of the vortex by the second mission (cf. Figs. 4-5). This was likely an important step in the intensity evolution of Earl, as a vertically-aligned vortex has a deeper, more well-developed secondary circulation that can effectively converge angular momentum surfaces and amplify the vortex (e.g., Ooyama 1982, Zehr 2003, Riemer et al. 2010). For the late stage, the primary question raised here was the processes that caused the CB's to be located inside the RMW for this rapidly intensifying hurricane. Additional work is needed, including more extensive sampling of the thermodynamic environment outside the RMW, coupled with high-resolution numerical modeling studies, to adequately address these questions.

REFERENCES

Black, M. L., J. F. Gamache, F. D. Marks, C. E. Samsury, and H. E. Willoughby, 2002: Eastern Pacific Hurricanes Jimena of 1991 and Olivia of 1994: The effect of vertical shear on structure and intensity. Mon. Wea. Rev., 130, 2291–2312.

Braun, S.A., and Coauthors, 2013: NASA's Genesis and Rapid Intensification Processes (GRIP) Field Experiment. Bull. Amer. Meteor. Soc., 94, 345–363.

Cecil, D. J., E. J. Zipser, and S. W. Nesbitt, 2002: Reflectivity, ice scattering, and lightning characteristics of hurricane eyewalls and rainbands. Part I: Quantitative description. Mon. Wea. Rev., 130, 769–784. Chen, H., and D. L. Zhang, 2013: On the rapid intensification of Hurricane Wilma (2005). Part II: Convective bursts and the upper-level warm core. J. Atmos. Sci., 70, 146–162.

DeHart, J.C., R.A. Houze, Jr., and R.F. Rogers, 2014: Quadrant distribution of tropical cyclone inner-core kinematics in relation to environmental shear. J. Atmos. Sci. Early online release, doi: http://dx.doi.org/10.1175/JAS-D-13-0298.1

DeMaria, M., M. Mainelli, L. K. Shay, J. A. Knaff, and J. Kaplan, 2005: Further improvements to the Statistical Hurricane Intensity Prediction Scheme (SHIPS). Wea. Forecasting, 20, 531–543.

Gamache, J. F., 1997: Evaluation of a fully three-dimensional variational Doppler analysis technique. Preprints, 28th Conf. on Radar Meteorology, Austin, TX, Amer. Meteor. Soc., 422–423.

Guimond, S. R., G. M. Heymsfield, and F. J. Turk, 2010: Multiscale observations of Hurricane Dennis (2005): The effects of hot towers on rapid intensification. J. Atmos. Sci., 67, 633–654.

Hazelton, A.T., and R.E. Hart, 2013: Hurricane Eyewall Slope as Determined from Airborne Radar Reflectivity Data: Composites and Case Studies. Wea. Forecasting, 28, 368–386.

Hazelton, A.T., R.F. Rogers, and R.E. Hart, 2014: Quantifying shear-relative asymmetries in tropical cyclone eyewall slope. To be submitted to Mon. Wea. Rev.

Hendricks, E. A., M. S. Peng, B. Fu, and T. Li, 2010: Quantifying environmental control on tropical cyclone intensity change. Mon. Wea. Rev., 138, 3243–3271.

Heymsfield, G. M., J. B. Halverson, J. Simpson, L. Tian, and T. P. Bui, 2001: ER-2 Doppler radar investigations of the eyewall of Hurricane Bonnie during the Convection and Moisture Experiment-3. J. Appl. Meteor., 40, 1310–1330.

Jones, S. C., 1995: The evolution of vortices in vertical shear. I: Initially barotropic vortices. Quart. J. Roy. Meteor. Soc., 121, 821–851.

Kaplan, J., M. DeMaria, and J. A. Knaff, 2010: A revised tropical cyclone rapid intensification index for the Atlantic and eastern North Pacific basins. Wea. Forecasting, 25, 220–241.

Kelley, O. A., J. Stout, and J. B. Halverson, 2004: Tall precipitation cells in tropical cyclone eyewalls are associated with tropical cyclone intensification. Geophys. Res. Lett., 31, L24112, doi:10.1029/2004GL021616.

Kepert, J. D., 2001: The dynamics of boundary layer jets within the tropical cyclone core. Part I: Linear theory. J. Atmos. Sci., 58, 2469–2484.

Marks, F. D., Jr., and L. K. Shay, 1998: Landfalling tropical cyclones: Forecast problems and associated research opportunities. Bull. Amer. Meteor. Soc., 79, 305–323.

Montgomery, M.T., J.A. Zhang, and R.K. Smith, 2014: An analysis of the observed low-level structure of rapidly intensifying and mature Hurricane Earl (2010). Quart. Jour. Roy. Met. Soc., in press.

Nolan, D. S., Y. Moon, and D. P. Stern, 2007: Tropical cyclone intensification from asymmetric convection: Energetics and efficiency. J. Atmos. Sci., 64, 3377–3405.

Ooyama, K., 1982: Conceptual evolution of the theory and modeling of the tropical cyclone. J. Meteor. Soc. Japan, 60, 369–380.

Pendergrass, A. G., and H. E. Willoughby, 2009: Diabatically induced secondary flows in tropical cyclones. Part I: Quasi-steady forcing. Mon. Wea. Rev., 137, 805–821.

Reasor, P. D., and M. D. Eastin, 2012: Rapidly intensifying Hurricane Guillermo (1997). Part II: Resilience in shear. Mon. Wea. Rev., 140, 425–444.

Reasor, P. D., R. F. Rogers, and S. Lorsolo, 2013: Environmental flow impacts on tropical cyclone structure diagnosed from airborne Doppler radar composites. Mon. Wea. Rev.,141, 2949–2969

Reasor, P. D., M. D. Eastin, and J. F. Gamache, 2009: Rapidly intensifying Hurricane Guillermo (1997). Part I: Low-wavenumber structure and evolution. Mon. Wea. Rev., 137, 603–631.

Riemer, M., M. T. Montgomery, and M. E. Nicholls, 2010: A new paradigm for intensity modification of tropical cyclones: Thermodynamic impact of vertical wind shear on the inflow layer. Atmos. Chem. Phys., 10, 3163–3188.

Rogers, R. F., S. Lorsolo, P. D. Reasor, J. Gamache, and F. D. Marks Jr., 2012: Multiscale analysis of tropical cyclone kinematic structure from airborne Doppler radar composites. Mon. Wea. Rev., 140, 77–99.

Rogers, R. F., and Coauthors, 2013a: NOAA's Hurricane Intensity Forecasting Experiment (IFEX): A progress report. Bull. Amer. Meteor. Soc.,94, 859–882. Schubert and Hack 1982

Rogers, R.F., P.D. Reasor, S. Lorsolo, 2013b: Airborne Doppler Observations of the Inner-Core Structural Differences between Intensifying and Steady-State Tropical Cyclones. Mon. Wea. Rev., 141, 2970–2991.

Shapiro, L.J., and H.E. Willoughby, 1982: The Response of Balanced Hurricanes to Local Sources of Heat and Momentum. J. Atmos. Sci., 39, 378–394.

Stern, D.P., D.S. Nolan, 2009: Reexamining the Vertical Structure of Tangential Winds in Tropical Cyclones: Observations and Theory. J. Atmos. Sci., 66, 3579–3600.

Uhlhorn, E.W., B.W. Klotz, T. Vukicevic, P.D. Reasor, and R.F. Rogers, 2014: Observed hurricane wind speed asymmetries and relationships to motion and environmental shear. Mon. Wea. Rev., 142, 1290-1311.

Vigh, J. L., and W. H. Schubert, 2009: Rapid development of the tropical cyclone warm core. J. Atmos. Sci., 66, 3335–3350.

Wang, Y., and G. J. Holland, 1996: Tropical cyclone motion and evolution in vertical shear. J. Atmos. Sci., 53, 3313–3332.

Zehr, R. M., 2003: Environmental vertical wind shear with Hurricane Bertha (1996). Wea. Forecasting, 18, 345–356.